Water Permeability of Aquaporin-4 Channel Depends on Bilayer Composition, Thickness, and Elasticity

Jihong Tong, Margaret M. Briggs, and Thomas J. McIntosh*
Department of Cell Biology, Duke University Medical Center, Durham, North Carolina

ABSTRACT Aquaporin-4 (AQP4) is the primary water channel in the mammalian brain, particularly abundant in astrocytes, whose plasma membranes normally contain high concentrations of cholesterol. Here we test the hypothesis that the water permeabilities of two naturally occurring isoforms (AQP4-M1 and AQP4-M23) depend on bilayer mechanical/structural properties modulated by cholesterol and phospholipid composition. Osmotic stress measurements were performed with proteoliposomes containing AQP4 and three different lipid mixtures: 1), phosphatidylcholine (PC) and phosphatidylglycerol (PG); 2), PC, PG, with 40 mol % cholesterol; and 3), sphingomyelin (SM), PG, with 40 mol % cholesterol. The unit permeabilities of AQP4-M1 were $3.3 \pm 0.4 \times 10^{-13}$ cm^3/s (mean $\pm$ SE), $1.2 \pm 0.1 \times 10^{-13}$ cm^3/s, and $0.4 \pm 0.1 \times 10^{-13}$ cm^3/s in PC:PG, PC:PG:cholesterol, and SM:PG:cholesterol, respectively. The unit permeabilities of AQP4-M23 were $2.1 \pm 0.2 \times 10^{-13}$ cm^3/s, $0.8 \pm 0.1 \times 10^{-13}$ cm^3/s, and $0.3 \pm 0.1 \times 10^{-13}$ cm^3/s in PC:PG, PC:PG:cholesterol, and SM:PG:cholesterol, respectively. Thus, for each isoform the unit permeabilities strongly depended on bilayer composition and systematically decreased with increasing bilayer compressibility modulus and bilayer thickness. These observations suggest that altering lipid environment provides a means of regulating water channel permeability. Such permeability changes could have physiological consequences, because AQP4 water permeability would be reduced by its sequestration into SM:cholesterol-enriched raft microdomains. Conversely, under ischemic conditions astrocyte membrane cholesterol content decreases, which could increase AQP4 permeability.

INTRODUCTION

The functional properties of several types of ion channels are modified by the structural or material properties of the membrane bilayer (1–4). In particular, cholesterol, which regulates both the hydrophobic thickness and elasticity (compressibility) of bilayers (5–7), has been shown to alter the activity of volume-regulated anion channels (8,9), the activation of sodium channels (10), the function of other classes of voltage-gated potassium channels (Kv1.5) (11), and the conductance of inwardly rectifying potassium (Kir) channels (12).

In this study, we investigate whether bilayer elastic and structural properties can also modify the water permeability of aquaporin (AQP) channels that are specialized for the selective permeability of water across membranes driven by osmotic gradients (13–15). In many tissues, AQPs are critical for water distribution and cell volume control (15,16).

Here we focus on the permeability of aquaporin-4 (AQP4) for several reasons:

1. The crystal structure of AQP4 has been obtained and related to proposed models of water transport (17).
2. AQP4 is found in mammalian brain astrocytes (18,19), whose membranes normally have high concentrations of cholesterol (20–23) that decrease after cerebral ischemia (20).
3. AQP4 plays important roles in water homeostasis and normal brain functions (19,24–32), and is implicated in several pathological conditions (26,28,33,34).
4. The regulation of astrocyte membrane water permeability has been a primary area of research interest, with evidence for roles of subcellular trafficking that brings AQP4 into the plasma membrane, as well as contributions from metal ions, hormones, pharmacological agents, and protein phosphorylation (35–40).
5. As of this writing, there is a controversy concerning the functions of the naturally occurring AQP4 isoforms (M1 and M23) that are splice variants with M1 having an additional 22 amino acids at its N-terminus. Different groups have found differing results for the relative water permeabilities of M1 and M23 when they are expressed in cells: M1 $>$ M23 (27), or M1 $<$ M23 (41), or M1 $\sim$ M23 (42). Because of the potential role of intracellular AQP4 trafficking, Gunnarson et al. (36) emphasize the advantages of determining the individual channel permeability in well-defined proteoliposome reconstitution systems.

In terms of regulation by lipid properties, detergent extraction studies suggest that AQP4 might be located in raft microdomains (43,44), transient regions of the plasma membrane enriched in sphingomyelin and cholesterol (45,46) that are thicker and less compressible than surrounding membrane regions (5,7). Noël et al. (44) note "the interesting hypothesis that lipid rafts may participate in the regulation of the AQP4 channel." In this regard, it

Submitted July 16, 2012, and accepted for publication September 4, 2012.

*Correspondence: t.mcintosh@cellbio.duke.edu

Editor: Paulo Almeida.

0006-3495/12/11/1899/10 $2.00

http://dx.doi.org/10.1016/j.bpj.2012.09.025

has been shown that the activities of Kir2.1/Kir2.3 channels depend on their distribution between raft and nonraft domains (47).

To explore the relationship between AQP4 permeability and its lipid environment, here we determine the permeability of M1 and M23 isoforms of AQP4 reconstituted into bilayers with different phospholipid and cholesterol compositions. We include bilayers containing phospholipids with monounsaturated hydrocarbon chains and no cholesterol, as well as bilayers containing the high concentrations of sphingomyelin (with mostly saturated hydrocarbon chains) and cholesterol characteristic of raft microdomains (7,48–50). These bilayer compositions have a wide range of bilayer thicknesses and compressibility moduli (5,51), providing quantitative tests of how channel water permeability is modified by bilayer structural and elastic properties.

MATERIALS AND METHODS

Expression and purification of AQP4 isoforms

The rat AQP4 isoforms M1 and M23 were expressed in yeast by techniques known to produce functional AQP (52–54). Plasmids pYES10-His-AQP4-M1 and pYES10-His-AQP4-M23 were expressed in the protease-deficient *Saccharomyces cerevisiae* (*pep*4) yeast, and purified as described in Yukutake et al. (52) with some modification. All buffers were supplemented with an EDTA-free protease inhibitor cocktail (Roche, Indianapolis, IN). The membrane pellet after ultracentrifugation was solubilized in buffer A containing 100 mM K_2HPO_4, 10% glycerol, 200 mM NaCl, 5 mM 2-mercaptoethanol, and 2% *n*-octyl-D-glucopyranoside (OG; Affymetrix, Cleveland, OH). After removing insoluble material by ultracentrifugation, the solubilized proteins were adjusted to 20 mM imidazole and gently mixed overnight with Ni-NTA agarose beads. The beads were washed in a column with 50 mM imidazole in Buffer A, and bound AQP4 was eluted with 750 mM imidazole in Buffer A.

The protein concentration was measured with the BCA assay using a BSA standard (Thermo Scientific, Rockford, IL). The purity of AQP4 was determined by sodium dodecyl sulfate-polyacrylamide gel electrophoresis (SDS-PAGE) and Western blots using antibodies from Santa Cruz Biotechnology (Santa Cruz, CA). For SDS-PAGE, protein samples were mixed (1:1) with Laemmli sample buffer containing 10% SDS and analyzed with a 4–20% gel. Gels, stained with Sypro Ruby, imaged and analyzed using a BioChemi System with LabWorks 4.0 (UVP BioImaging System, Upland, CA), showed that the AQP4 was >90% pure.

Reconstitution of AQP4 into proteoliposomes

Palmitoyloleoyl phosphatidylcholine (POPC) ((C16:0)(C18:1)PC), palmitoyloleoyl phosphatidylglycerol (POPG) ((C16:0)(C18:1)PG), dipalmitoyl phosphatidylglycerol (DPPG) ((C16:0)(C16:0)PG), bovine brain sphingomyelin (SM), and cholesterol were purchased from Avanti Polar Lipids (Alabaster, AL). To obtain bilayers with a range of thicknesses and elastic properties, we used three specific lipid mixtures: POPC:POPG (8:2 M:M), POPC:POPG:cholesterol (4:2:4 M:M:M), and SM:DPPG:cholesterol (4:2:4 M:M:M). The negatively charged PGs, with hydrocarbon chain compositions similar to the accompanying choline-containing phospholipids, were included to help stabilize large unilamellar proteoliposomes and minimize aggregation. The lipids were mixed in chloroform:methanol, dried by rotary evaporation, and hydrated in 25 mM 4-(2-hydroxyethyl)-1-piperazineethanesulfonic acid (HEPES), 50 mM NaCl, 2% OG, pH 7.4.

To ensure complete hydration, the SM:DPPG:cholesterol specimens were hydrated at 40°C, whereas the other lipids were hydrated at 20°C. The lipids and proteins in OG were mixed at appropriate lipid/protein ratios, OG was removed by dialysis against 25 mM HEPES, 50 mM NaCl, 2 mM dithreitol (DTT), and 1 mM phenylmethanesulfonylfluoride or phenylmethylsulfonyl fluoride (PMSF), pH 7.4, initially for 4 h at room temperature followed by two days at room temperature for SM:DPPG:cholesterol or at 4°C for the other lipids. The resulting lipid/protein vesicles were collected by ultracentrifugation (55) and resuspended in dialysis buffer plus 50 mM sucrose. Large unilamellar proteoliposomes were obtained by extrusion through 100-nm pore filters (Avanti Polar Lipids).

For each sample, the average vesicle diameter was determined by quasielastic light scattering with a ZetaPlus Zeta Potential Analyzer (Brookhaven Instruments, Holtsville, NY), and ranged from 100 nm to 270 nm depending on the sample protein/lipid ratio. For some samples, the diameters were verified by electron microscopy of negative stained specimens or by cryo-transmission electron microscopy of unfixed specimens by NanoImaging Services (La Jolla, CA). The cryo-electron micrographs showed that >80% of the vesicles contained a single-wall, with some containing entrapped vesicles (see Fig. S1 in the Supporting Material). The AQP4 unit water permeabilities were independent of average vesicle diameter.

The lipid and protein compositions of the proteoliposomes were determined by phosphate assays (56) and SDS-PAGE, respectively. AQP4 in proteoliposomes and known amounts of AQP4 in OG (standardized by BCA assay) were analyzed on the same SDS gel. Integrated optical densities were measured, and the absolute AQP4 concentrations in proteoliposomes were calculated by comparison with the standards, which showed a linear response. This approach was necessary because the lipids interfered with direct BCA assays.

Measurements of AQP4-proteoliposome water permeability

Water permeabilities were measured using techniques that apply an osmotic gradient with sucrose solutions and determine as a function of time the change in proteoliposome volume due to water efflux (14,17,52,53,57–64). We measured the volume change by light scattering with a wavelength of 600 nm (61,62) using a SX20 Stopped-Flow Spectrometer (Applied Photophysics, Leatherhead, UK). The proteoliposome permeabilities (p_f), with units of cm/s, were calculated from the formula

$$p_f = \frac{k}{\{(SAV)(V_W)(C_{out} - C_{in})\}}, \quad (1)$$

where k is the shrinkage rate determined by exponential fits to the light-scattering data, SAV is the vesicle surface area/volume ratio, V_W is the partial molar volume of water (18 cm^3/mol), and C_{in} (50 mM) and C_{out} (150 mM) are the initial concentrations of solute inside and outside the vesicles (60,61). For proteoliposomes made from POPC:POPG or POPC:POPG:cholesterol, the time course was recorded from 0 to 5 s, whereas for the slower volume changes observed with proteoliposomes containing SM:DPPG:cholesterol, data were recorded from 0 to 10 s. The light-scattering data were fit using the software Logger Pro 3.8 (Vernier Software, Beaverton, OR).

The AQP4 single-channel unit permeabilities (P_u), with units of cm^3/s, were determined with the formula $P_u = p_f/S_{uD}$ (65), where S_{uD} is the AQP4 density per unit surface area. For each proteoliposome preparation, S_{uD} was calculated from the measured vesicle diameters, protein concentrations, lipid concentrations, and area per lipid molecule (A_m). For our lipid systems A_m was estimated from literature x-ray diffraction and monolayer data for PC, PC:cholesterol, and SM:cholesterol systems with the assumption that PGs with matching hydrocarbon chain compositions have approximately the same A_m as PCs. For POPC:POPG, we used $A_m = 0.66$ nm^2,

based on the A_m of POPC measured by x-ray diffraction at 30°C (66) extrapolated to 20°C with the thermal coefficient of area expansion for PC bilayers (67). To our knowledge, there are no direct x-ray measurements of A_m for POPC:cholesterol or SM:cholesterol bilayers. Therefore, because of the similarity of eggPC (5) and POPC (60) bilayers, for POPC:POPG:cholesterol we used $A_m = 0.47$ nm^2 measured by x-ray diffraction for eggPC:cholesterol (6:4) bilayers (6). For SM:DPPG:cholesterol, we used $A_m = 0.42$ nm^2, based on monolayer data showing for a range of surface pressures that the A_m of SM:cholesterol (6:4) is ~90% that of POPC:cholesterol (6:4) (68).

RESULTS

Fig. 1 shows typical osmotic gradient-driven changes in the time course of light scattering for POPC:POPG single-walled vesicles in the presence and absence of AQP4-M1. For both traces, the light scattering increased sharply after the osmotic gradient was applied at time $t = 0$ and eventually leveled off. Both traces could be fit closely to a single-exponential function, and, in the absence of protein, our measured values of liposome water permeability were similar to previously reported values (see the Supporting Material). However, the rate of change in light scattering was increased by the presence of AQP4-M1 (Fig. 1), indicating that it increased the water permeability of the vesicle.

Representative changes in light scattering for proteoliposomes containing similar concentrations of AQP4-M1 in bilayers of different lipid compositions are shown in Fig. 2. The rate of scattering increase depended strongly on the lipid system, being fastest for POPC:POPG, slower for POPC:POPG:cholesterol, and slowest for SM:DPPG:cholesterol. For each sample of POPC:POPG and POPC:POPG:cholesterol, data (such as those shown in Fig. 2) could be closely fit (root-mean-square errors between 0.03 and 0.06) with a single-exponential rise, yielding a single value of p_f for each specimen. Likewise, for SM:DPPG:cholesterol liposomes in the absence of protein, the data could be fit with a single exponential. However, for SM:DPPG:cholesterol proteoliposomes, a double-exponential fit was required to obtain equivalent root-mean-square error (Fig. 2), yielding two sets of p_f, a larger one that increased with increasing P/L, as well as a much smaller one that was independent of P/L and had similar values to the control SM:DPPG:cholesterol liposomes ($P/L = 0$). For subsequent analysis with this lipid system, we used the larger values of p_f that increased with increasing P/L.

Similar experiments were used with Eq. 1 to calculate p_f for both AQP4-M1 and AQP4-M23 over broad ranges of protein-lipid (P/L) ratios (Fig. 3, *A* and *B*). For both isoforms, and with all three lipid systems, the

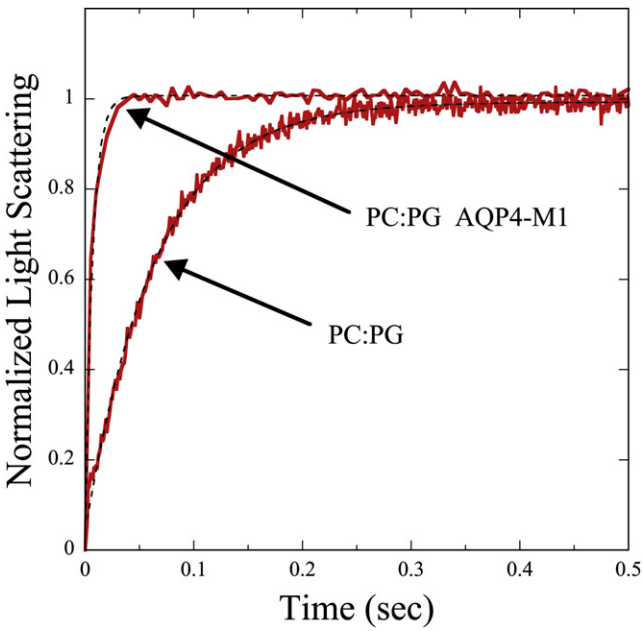

FIGURE 1 Osmotic gradient-driven changes in light scattering for POPC:POPG bilayers in the absence of protein or with AQP4-M1 at a P/L ratio of 0.0023. Data (*red*), with single-exponential fits (*black dotted lines*). For both systems the osmotic gradient was applied at time $t = 0$ and the traces were put on the same relative scale by normalizing the light scattering to go from 0 at time $t = 0$ to 1 when the scattering leveled off. The values of k were determined to be 15.5 s^{-1} for POPC:POPG liposomes and 120.5 s^{-1} for POPC:POPG proteoliposomes containing AQP4-M1.

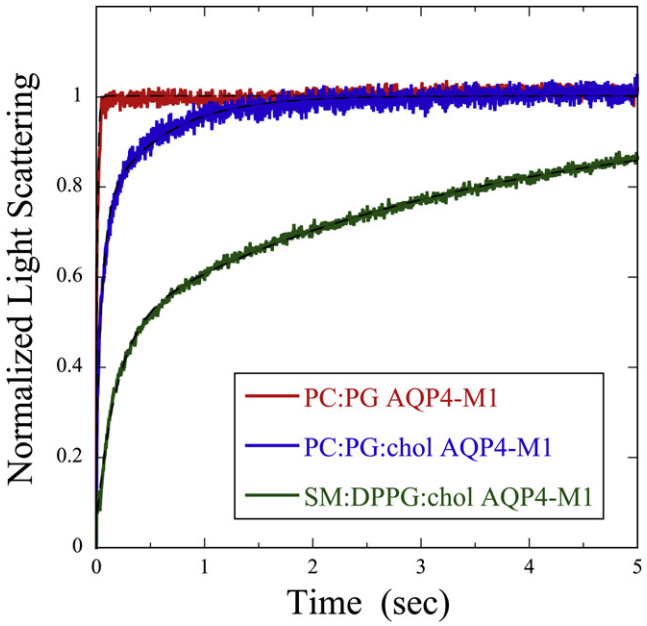

FIGURE 2 Osmotic gradient-driven changes in light scattering for proteoliposomes containing AQP4-M1 at similar molar protein/lipid ratios: POPC:POPG ($P/L = 0.0023$) (*red trace*), POPC:POPG:cholesterol ($P/L = 0.0018$) (*blue trace*), and SM:DPPG:cholesterol ($P/L = 0.0015$) (*green trace*). The traces were normalized as in Fig. 1 and fits are shown (*black dotted lines*). Although data were recorded for a 10-s time interval for proteoliposomes containing SM:DPPG:cholesterol, the light-scattering data are displayed for only the first 5 s to better show the differences among the three lipid systems. From these traces, the values of k were determined to be 120.5 s^{-1} for POPC:POPG proteoliposomes and 47.3 s^{-1} for POPC:POPG:cholesterol proteoliposomes. For the SM:DPPG:cholesterol proteoliposomes, the two values of k were 5.0 s^{-1} and 0.2 s^{-1}.

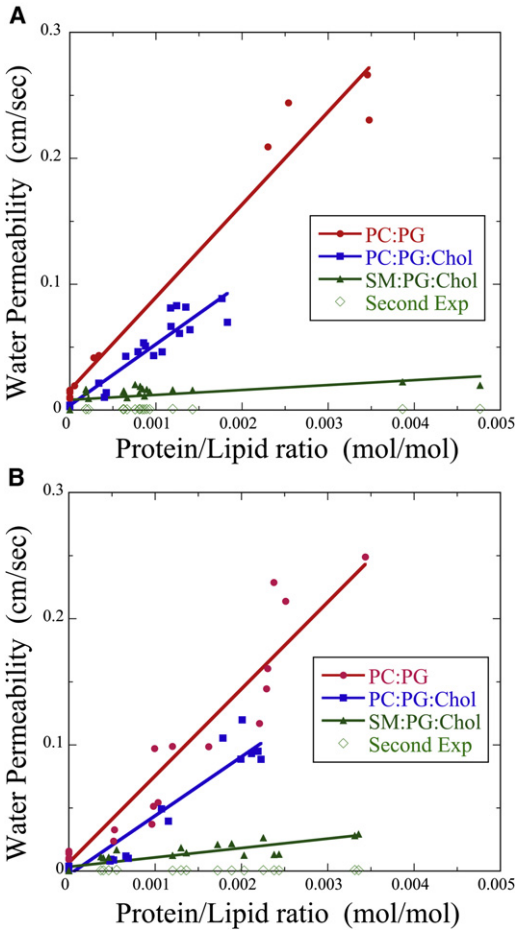

FIGURE 3 Plots of p_f as a function of protein/lipid ratio (M/M) for AQP4-M1 (*A*) and AQP4-M23 (*B*) in bilayers composed of POPC:POPG (8:2) (*red circles*), POPC:POPG:cholesterol (4:2:4) (*blue squares*), and SM:DPPG:cholesterol (4:2:4) (*green triangles* and *green diamonds*). For proteoliposomes made with POPC:POPG or POPC:POPG:cholesterol, each osmotic gradient run yielded a single value of k, and therefore a single value of p_f that increased with increasing P/L ratio. For each SM:DPPG:cholesterol proteosome, the osmotic gradient yielded two values of k: one gave p_f that increased with increasing P/L (*green triangles*), whereas the other gave p_f that stayed nearly constant as a function of P/L (*green diamonds*) and had similar magnitudes to SM:DPPG:cholesterol liposomes ($P/L = 0$).

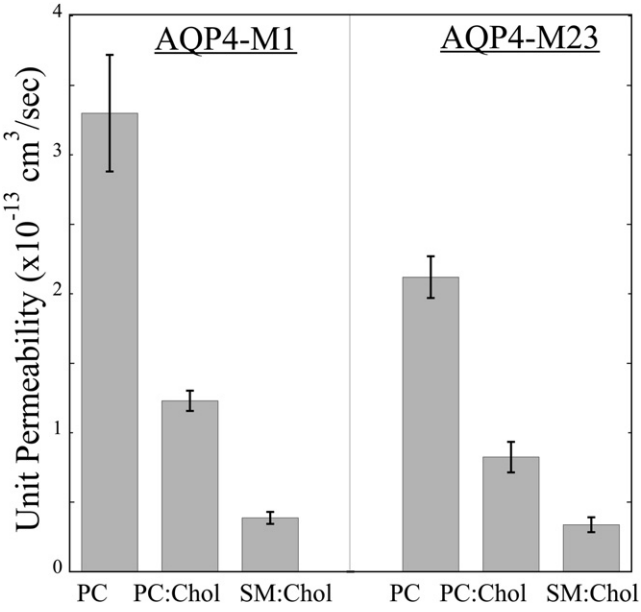

FIGURE 4 Single-channel (unit) permeabilities (mean ± SE) of AQP4-M1 and AQP4-M23 isoforms in bilayers with the lipid compositions shown in Fig. 3. (For simplicity, the lipid labels on the x axis do not include the relevant PG.)

proteoliposome water permeability increased linearly with increasing P/L ratio. For both AQP4 isoforms, p_f depended strongly on the composition of the lipid bilayer and varied in the order POPC:POPG > POPC:POPG:cholesterol > SM:DPPG:cholesterol.

Using the p_f data (Fig. 3) along with vesicle sizes and lipid areas per molecule, we calculated the single-channel (unit) permeability (P_u) for both AQP4-M1 and AQP4-M23 isoforms for the three different lipid systems. As shown in Fig. 4, for each isoform P_u depended strongly on the composition of the lipid bilayer, with the differences being statistically significant: POPC:POPG > POPC:POPG:cholesterol (P values = 0.011 and 0.001 for AQP4-M1 and AQP4-M23, respectively), POPC:POPG:cholesterol > SM:DPPG:cholesterol (P = 0.020 and 0.008), and POPC:POPG > SM:DPPG:cholesterol ($P = 0.005$ for both isoforms).

To assess whether the differences between lipid compositions shown in Fig. 4 are related to differences in either bilayer mechanical or structural properties, we plot in Fig. 5 the unit permeabilities versus the square root of the bilayer area compressibility moduli ($K_A^{1/2}$), a direct measure of bilayer elastic properties, and bilayer hydrocarbon thickness (d_{hc}). We use $K_A^{1/2}$ in Fig. 5 *A* because it has been experimentally shown for one-component PC bilayers that elastic bending (k_c) and area compressibility moduli are related to bilayer hydrocarbon thickness (d_{hc}) by the relation $(k_c/K_A)^{1/2} \propto d_{hc}$ (69).

Values of K_A were calculated based on recent measurements in similar lipid systems where corrections were made for bilayer undulations (5,69). For POPC:POPG (8:2) we used K_A of the analogous lipid 1-stearoyl-2-oleoyl-*sn*-glycero-3-phosphatidylcholine (SOPC) (5), for POPC:POPG:cholesterol (4:2:4) we used the K_A measured for SOPC:cholesterol (1:1) (5) modified by a correction factor of 0.6 taking into account the difference between SOPC bilayers containing 50 and 40 mol % cholesterol (see Fig. 3 of Needham and Nunn (51)), and for SM:DPPG:cholesterol (4:2:4) we used K_A of SM:cholesterol (1:1) (5) with the same correction factor of 0.6. In terms of d_{hc}, for POPC:POPG we used d_{hc} measured for POPC (66), for POPC:POPG:cholesterol we used d_{hc} of SOPC:cholesterol (70), and for SM:DPPG:cholesterol we used d_{hc} of SM:cholesterol (7). For both AQP4-M1 and

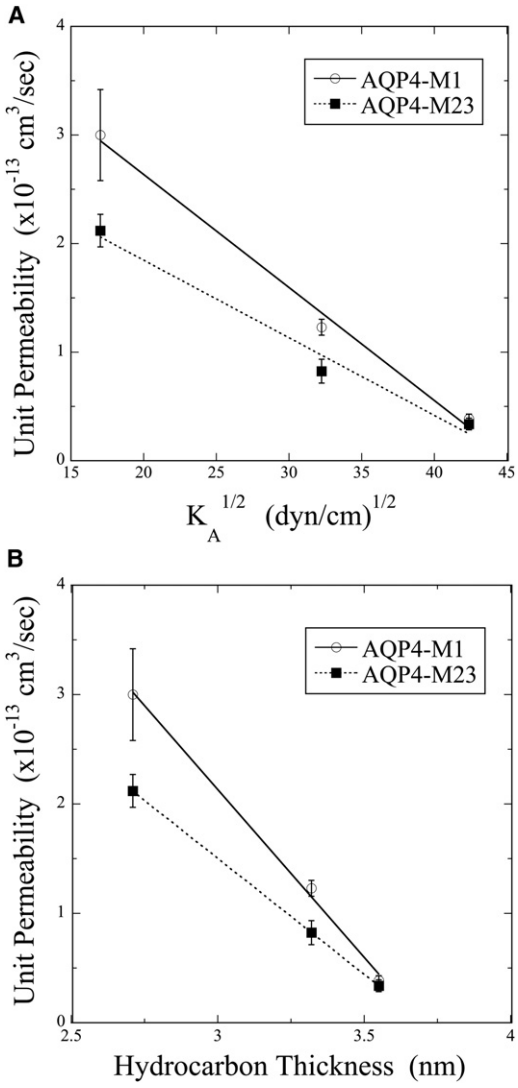

FIGURE 5 Unit permeabilities of AQP4-M1 and AQP4-M23 plotted against the square-root of bilayer area compressibility modulus ($K_A^{1/2}$) (*A*) and bilayer hydrocarbon thickness (d_{hc}) (*B*) with linear fits to the data.

AQP4-M23, P_u decreased linearly with increasing values of either $K_A^{1/2}$ (Fig. 5 *A*) or d_{hc} (Fig. 5 *B*).

DISCUSSION

The data presented in this report show that the water permeability of individual AQP4 channels strongly depended on the structural and mechanical properties of the membrane bilayer matrix as modified by both cholesterol content and phospholipid hydrocarbon chain composition.

Liposome and proteoliposome permeabilities

In the absence of protein, our values for the water permeabilities of liposomes (i.e., large unilamellar vesicles) are similar to values reported for similar lipid systems (71–73) (see the Supporting Material). Although many factors could contribute, Mathai et al. (73) conclude that this bilayer water leakage should strongly correlate with the area per lipid molecule, as also found for our data (see Fig. S2).

There have been several previous measurements of p_f for proteoliposomes containing various AQPs, including AQP1 (14,57), AQP2 (65,74), AQP4 (52,61,62), AQP8 (53), AQP9 (63), AQPZ (60), and AQPM (54). Many of these experiments used bilayers primarily containing bacterial lipids, although some have been done in phospholipids with smaller concentrations of cholesterol than used here (14,62). To the best of our knowledge, no previous experiments have been performed with rigid bilayers containing SM and cholesterol. To obtain a good fit to the light-scattering data for SM:DPPG:cholesterol proteoliposomes (such as shown in Fig. 2), it was necessary to use the sum of two exponential functions, which previously has been done for some AQP-containing proteoliposomes (63). In the specimen shown in Fig. 2, we found the two values of k to be $k_1 = 5.0\ s^{-1}$ and $k_2 = 0.2\ s^{-1}$.

We realize that k_2 is not as accurately determined as k_1 because the data were collected over a time period of 10 s, or only about twice the characteristic time period of the second exponential ($1/k_2 = 5$ s). Nonetheless, it seems likely that the faster exponential rise (k_1) represents water permeability through the AQP4 channel, whereas the slower exponential rise (k_2) is probably due to water leaking through the bilayer matrix, perhaps exacerbated by an inhomogeneous protein-lipid distribution among the proteoliposomes. Two pieces of evidence support this bilayer leakage explanation for the slower exponential rise. First, for the slower exponential function, the p_f values were independent of protein/lipid ratio and similar to SM:DPPG:cholesterol liposomes (Fig. 3), whereas for the faster exponential rise, the values of p_f increased linearly with increasing protein/lipid ratio. Second, only one exponential was needed for AQP4 in either POPC:POPG or POPC:POPG:cholesterol where the AQP4 unit permeabilities were much larger than those in SM:DPPG:cholesterol (Fig. 4). That is, the background bilayer leakage was small in comparison to the AQP4 channel permeability in POPC:POPG or POPC:POPG:cholesterol bilayers, but not in SM:DPPG:cholesterol bilayers.

For each lipid system examined here (Fig. 3), p_f-versus-protein/lipid relationships followed a straight line, which has previously been found for AQP1 (channel-forming integral protein) in *Escherichia coli* lipids (14) (when protein/vesicle in their Fig. 3 *E* is converted to protein/lipid). For one concentration of AQP1, Zeidel et al. (14) found p_f to be the same in *E. coli* lipids containing 0, 5, or 15% cholesterol. This is not surprising, as these relatively small amounts of cholesterol would not be expected to markedly alter the elastic properties of the bilayer (51).

AQP4 channel unit permeabilities

There have been relatively few measurements of P_u for AQPs reconstituted in proteoliposomes. For AQP4-M23, Yang et al. (62) recorded $P_u = 1.5 \times 10^{-13}$ cm^3/s in bilayers of DPPC: phosphatidylethanolamine: phosphatidylinositol: cholesterol (4.5:2.3:0.5:2.7), which is between our measured values of $P_u = 3.3 \times 10^{-13}$ cm^3/s in POPC: POPG (8:2) and $P_u = 1.2 \pm 0.1 \times 10^{-13}$ cm^3/s in POPC: POPG:cholesterol (4:2:4). Because Yang et al. (62) used a system with a cholesterol concentration between that of our POPC:POPG and POPC:POPG:cholesterol bilayers, it is quite reasonable that their value of P_u falls between our values.

For each of our lipid systems, the unit permeability was larger for AQP4-M1 than for AQP4-M23 (Fig. 4). The difference was statistically significant for both POPC: POPG (P value $= 0.014$) and POPC:POPG:cholesterol ($P = 0.003$), but not statistically significant for SM:DPPG: cholesterol ($P = 0.231$). Our data do not address the contribution of orthogonal array formation of the M23 isoform (75,76), which remains to be explored.

The value of $P_u = 4.6 \times 10^{-14}$ cm^3/s measured for AQP1 (channel-forming integral protein) in proteoliposomes composed of *E. coli* lipids (14) is considerably smaller than our AQP4 values measured either in POPC:POPG or POPC:POPG:cholesterol (Fig. 4), but comparable to our values measured for the AQP4 isoforms in SM:DPPG: cholesterol proteoliposome. Although the thickness and compressibility modulus have not been measured for the *E. coli* lipids, because they contain phospholipids with double bonds and no cholesterol, it would be expected that its d_{hc} and K_A are more similar to that of POPC:POPG than to those of POPC:POPG:cholesterol or SM:DPPG: cholesterol. This suggests that P_u for AQP4 is greater than for AQP1 in similar lipids, consistent with comparisons of these AQPs expressed in oocytes (77).

Possible mechanisms of bilayer influences on AQP4 permeability

We now consider possible mechanisms by which changes in bilayer lipid composition modified the AQP4 single-channel permeability (Fig. 5). Both theoretical treatments (78–81) and experimental studies (80–83) indicate that bilayer structural and material properties can affect protein confirmation and activity, with the elastic and structural properties interrelated (84,85). As noted by Lundbaek et al. (86), there is a hydrophobic coupling of protein function to bilayer material properties so that "the bilayer becomes an allosteric regulator of membrane protein function."

Insights on the role of elastic properties can be obtained from comparisons of crystal structures of AQP0 in detergent micelles (by x-ray crystallography of three-dimensional crystals) and lipid bilayers (by electron microscopy of two-dimensional crystals) (87–89). In the two environments, AQP0 displays differences in temperature factors.

As noted by Hite et al. (90),

> "The higher temperature factors of the detergent-exposed atoms in the x-ray structures indicate that the detergent molecules do not restrict their conformational variability as much as the lipid molecules do. A possible explanation for this observation is that the contacts in the three-dimensional crystal are mainly formed by the soluble, extramembranous loops, whereas the residues contacting the lipids in the two-dimensional crystals are an integral part of the crystal contacts. An alternative explanation would be the lateral pressure from the lipids that could restrict the conformational flexibility of the entire transmembrane domain."

This alternative explanation might help explain the dependence of AQP4 P_u on bilayer composition (Fig. 5), as the lateral pressure profile depends on bilayer cholesterol content (91,92) and phospholipid hydrocarbon chain unsaturation (92,93,95). It has also recently been shown that lipid acyl chains, rather than lipid headgroups, determine the lipid localization around AQP0 (96).

Bilayer width plays a role in protein activity due to hydrophobic-mismatch between protein hydrophobic length and bilayer hydrocarbon thickness (d_{hc}) (4,84,85,97–101). A hydrophobic coupling between protein and surrounding bilayer exists due to the high cost of exposing either hydrophobic amino-acid residues or lipid acyl chains to the aqueous environment (4,78,102). To avoid this hydrophobic mismatch there is either a change in protein conformation or local bilayer thickness. Therefore, changes in the physical properties of the bilayer alter the protein conformational equilibrium and function (103).

Experiments have shown that hydrophobic mismatch affects the activity of melibiose transporters (101), BK calcium channels (84), and mechanosensitive ion channels (85). In terms of AQP water channels, in AQP0 crystals containing dimyristoyl phosphatidylcholine (DMPC) the width of the hydrocarbon region of the DMPC bilayer is ~2.4 nm (90), and the length of the AQP4 conducting pore is ~2.5 nm (17). These values are closer to d_{hc} for POPC:POPG (2.7 nm) than for POPC:POPG:cholesterol (3.3 nm) or SM:DPPG:cholesterol (3.6 nm) (Fig. 5 *B*). Thus, for our lipid systems, the hydrophobic-mismatch between AQP4 hydrophobic length and d_{hc} varies in the order SM:DPPG:cholesterol > POPC:POPG:cholesterol > POPC:POPG, consistent with our observed differences in P_u.

Therefore, we argue that small AQP4 transmembrane conformational changes resulting from differences in bilayer composition could modify the single-file movement of water molecules through the narrow (0.15-nm diameter) channel observed in AQP4 crystals (17). The results (Fig. 5, *A* and *B*) indicate that nonspecific interactions

play major roles; future experiments will be designed to sort out the relative contributions of bilayer elasticity and bilayer thickness.

Specific cholesterol-protein interactions have also been shown to modify the function of some membrane channels (1,12,104). However, we argue that potential specific cholesterol-AQP4 interactions do not make a dominant contribution to the total effect because, for the same protein/cholesterol ratio, the observed P_f is quite different for POPC:POPG:cholesterol and SM:DPPG:cholesterol bilayers (Fig. 3).

Physiological significance of these results

Our observation that AQP4 permeability depends on its lipid environment could have biological relevance in both health and disease. In terms of normal glial cells, the partitioning of either AQP4 isoform from nonraft-membrane microdomains (with relatively little cholesterol) into raft microdomains (enriched in SM and cholesterol) would significantly reduce its water permeability. As noted in the Introduction, AQP4 is thought to be enriched in rafts, with basal lamina and cytoplasmic proteins involved in its raft incorporation (24,43,44).

Moreover, each AQP4 isoform has properties that could further promote its sequestration into rafts. Specifically, the N-terminus of M1 contains two cysteine residues that can be palmitoylated (105), a process that promotes protein incorporation into rafts (106,107). The AQP4-M23 isoform forms regular orthogonal arrays in membranes (108,109), and the homooligomerization of another AQP (AQP0) has been shown to increase its partitioning into raft bilayers (55). Thus, we suggest that there are different posttranslational modifications that could potentially bring each AQP4 isoform into raft microdomains and thereby regulate its water permeability properties in membranes.

Astrocyte end-feet processes compose a part of the boundary between blood vessels and nervous tissue in the central nervous system. This blood-brain barrier restricts the movement into the brain of many substances that in other tissues normally leave blood vessels and diffuse into the tissues. In multiple sclerosis and animal models such as experimental autoimmune encephalomyelitis, dysfunction of this barrier leads to brain edema (110–112). It has recently been found that during experimental autoimmune encephalomyelitis (113) and in high-grade astrocytomas (114), there is a loss of the polarized location of AQP4 in astrocyte end-feet. We raise the possibility that there may be a different lipid composition in end-feet membranes than in membranes in the rest of the cell that could modify AQP4 function. Future experiments are necessary to test these concepts.

SUPPORTING MATERIAL

Two figures and one table are available at http://www.biophysj.org/biophysj/supplemental/S0006-3495(12)01062-4.

We thank Dr. Peter Agre for supplying plasmids, Dr. Yangjian Liu and Dr. Kun Liu for assistance with AQP4 expression and purification, Dr. Harold Erickson for the use of the French press, Dr. Terrence Oas for use of the stopped-flow apparatus, Dr. David Needham for use of the quasielastic light-scattering equipment, and Dr. R. J. Perz-Edwards and Ms. Susan Hester for negative stain electron microscopy experiments. We also thank Drs. Jennifer Carbrey, Sid Simon, Evan Evans, and Joe Corless for many helpful suggestions.

This work was supported by grant No. GM27278 from the National Institutes of Health, Bethesda, Maryland.

REFERENCES

1. Levitan, I., Y. Fang, …, V. Romanenko. 2010. Cholesterol and ion channels. *Subcell. Biochem.* 51:509–549.
2. McIntosh, T. J., and S. A. Simon. 2006. Roles of bilayer material properties in function and distribution of membrane proteins. *Annu. Rev. Biophys. Biomol. Struct.* 35:177–198.
3. Phillips, R., T. Ursell, …, P. Sens. 2009. Emerging roles for lipids in shaping membrane-protein function. *Nature.* 459:379–385.
4. Andersen, O. S., and R. E. Koeppe, 2nd. 2007. Bilayer thickness and membrane protein function: an energetic perspective. *Annu. Rev. Biophys. Biomol. Struct.* 36:107–130.
5. Rawicz, W., B. A. Smith, …, E. Evans. 2008. Elasticity, strength, and water permeability of bilayers that contain raft microdomain-forming lipids. *Biophys. J.* 94:4725–4736.
6. Lecuyer, H., and D. G. Dervichian. 1969. Structure of aqueous mixtures of lecithin and cholesterol. *J. Mol. Biol.* 45:39–57.
7. Gandhavadi, M., D. Allende, …, T. J. McIntosh. 2002. Structure, composition, and peptide binding properties of detergent soluble bilayers and detergent resistant rafts. *Biophys. J.* 82:1469–1482.
8. Byfield, F. J., B. D. Hoffman, …, I. Levitan. 2006. Evidence for the role of cell stiffness in modulation of volume-regulated anion channels. *Acta Physiol. (Oxf.).* 187:285–294.
9. Levitan, I., A. E. Christian, …, G. H. Rothblat. 2000. Membrane cholesterol content modulates activation of volume-regulated anion current in bovine endothelial cells. *J. Gen. Physiol.* 115:405–416.
10. Lundbaek, J. A., P. Birn, …, O. S. Andersen. 2004. Regulation of sodium channel function by bilayer elasticity: the importance of hydrophobic coupling. Effects of micelle-forming amphiphiles and cholesterol. *J. Gen. Physiol.* 123:599–621.
11. Abi-Char, J., A. Maguy, …, S. N. Hatem. 2007. Membrane cholesterol modulates Kv1.5 potassium channel distribution and function in rat cardiomyocytes. *J. Physiol.* 582:1205–1217.
12. Romanenko, V. G., G. H. Rothblat, and I. Levitan. 2002. Modulation of endothelial inward-rectifier K^+ current by optical isomers of cholesterol. *Biophys. J.* 83:3211–3222.
13. Agre, P., G. M. Preston, …, S. Nielsen. 1993. Aquaporin CHIP: the archetypal molecular water channel. *Am. J. Physiol.* 265:F463–F476.
14. Zeidel, M. L., S. Nielsen, …, P. Agre. 1994. Ultrastructure, pharmacologic inhibition, and transport selectivity of aquaporin channel-forming integral protein in proteoliposomes. *Biochemistry.* 33:1606–1615.
15. Agre, P., and D. Kozono. 2003. Aquaporin water channels: molecular mechanisms for human diseases. *FEBS Lett.* 555:72–78.
16. King, L. S., D. Kozono, and P. Agre. 2004. From structure to disease: the evolving tale of aquaporin biology. *Nat. Rev. Mol. Cell Biol.* 5:687–698.
17. Ho, J. D., R. Yeh, …, R. M. Stroud. 2009. Crystal structure of human aquaporin 4 at 1.8 Å and its mechanism of conductance. *Proc. Natl. Acad. Sci. USA.* 106:7437–7442.
18. Hiroaki, Y., K. Tani, …, Y. Fujiyoshi. 2006. Implications of the aquaporin-4 structure on array formation and cell adhesion. *J. Mol. Biol.* 355:628–639.

19. Jung, J. S., R. V. Bhat, …, P. Agre. 1994. Molecular characterization of an aquaporin cDNA from brain: candidate osmoreceptor and regulator of water balance. *Proc. Natl. Acad. Sci. USA*. 91:13052–13056.
20. Cuevas, P., J. A. Gutierrez-Diaz, …, J. I. Ausman. 1987. Intramembranous cytochemistry: a new morphological technique for studying cholesterol in the astrocyte plasma membrane of ischemic brain cells. *Neurosurgery.* 20:243–248.
21. Gotow, T. 1984. Cytochemical characteristics of astrocytic plasma membranes specialized with numerous orthogonal arrays. *J. Neurocytol.* 13:431–448.
22. Liu, J. P., Y. Tang, …, H. Li. 2010. Cholesterol involvement in the pathogenesis of neurodegenerative diseases. *Mol. Cell. Neurosci.* 43:33–42.
23. Mauch, D. H., K. Nägler, …, F. W. Pfrieger. 2001. CNS synaptogenesis promoted by glia-derived cholesterol. *Science.* 294:1354–1357.
24. Amiry-Moghaddam, M., A. Williamson, …, O. P. Ottersen. 2003. Delayed K^+ clearance associated with aquaporin-4 mislocalization: phenotypic defects in brains of α-syntrophin-null mice. *Proc. Natl. Acad. Sci. USA*. 100:13615–13620.
25. Benfenati, V., M. Caprini, …, M. Amiry-Moghaddam. 2011. An aquaporin-4/transient receptor potential vanilloid 4 (AQP4/TRPV4) complex is essential for cell-volume control in astrocytes. *Proc. Natl. Acad. Sci. USA*. 108:2563–2568.
26. Bloch, O., and G. T. Manley. 2007. The role of aquaporin-4 in cerebral water transport and edema. *Neurosurg. Focus*. 22:E3.
27. Fenton, R. A., H. B. Moeller, …, N. MacAulay. 2010. Differential water permeability and regulation of three aquaporin-4 isoforms. *Cell. Mol. Life Sci.* 67:829–840.
28. Manley, G. T., D. K. Binder, …, A. S. Verkman. 2004. New insights into water transport and edema in the central nervous system from phenotype analysis of aquaporin-4 null mice. *Neuroscience.* 129:983–991.
29. Nicchia, G. P., M. Srinivas, …, D. C. Spray. 2005. New possible roles for aquaporin-4 in astrocytes: cell cytoskeleton and functional relationship with connexin43. *FASEB J.* 19:1674–1676.
30. Pasantes-Morales, H., and S. Cruz-Rangel. 2010. Brain volume regulation: osmolytes and aquaporin perspectives. *Neuroscience.* 168:871–884.
31. Verkman, A. S., D. K. Binder, …, M. C. Papadopoulos. 2006. Three distinct roles of aquaporin-4 in brain function revealed by knockout mice. *Biochim. Biophys. Acta.* 1758:1085–1093.
32. Badaut, J., J. F. Brunet, and L. Regli. 2007. Aquaporins in the brain: from aqueduct to "multi-duct". *Metab. Brain Dis.* 22:251–263.
33. Frydenlund, D. S., A. Bhardwaj, …, M. Amiry-Moghaddam. 2006. Temporary loss of perivascular aquaporin-4 in neocortex after transient middle cerebral artery occlusion in mice. *Proc. Natl. Acad. Sci. USA*. 103:13532–13536.
34. Saini, H., G. Fernandez, …, M. Levy. 2010. Differential expression of aquaporin-4 isoforms localizes with Neuromyelitis optica disease activity. *J. Neuroimmunol.* 221:68–72.
35. Gunnarson, E., M. Zelenina, and A. Aperia. 2004. Regulation of brain aquaporins. *Neuroscience.* 129:947–955.
36. Gunnarson, E., M. Zelenina, …, A. Aperia. 2008. Identification of a molecular target for glutamate regulation of astrocyte water permeability. *Glia.* 56:587–596.
37. Noell, S., P. Fallier-Becker, …, H. Wolburg. 2007. Effects of agrin on the expression and distribution of the water channel protein aquaporin-4 and volume regulation in cultured astrocytes. *Eur. J. Neurosci.* 26:2109–2118.
38. Qing, W. G., Y. Q. Dong, …, P. Y. Heng. 2009. Brain edema after intracerebral hemorrhage in rats: the role of iron overload and aquaporin 4. *J. Neurosurg.* 110:462–468.
39. Yukutake, Y., Y. Hirano, …, M. Yasui. 2009. Rapid and reversible inhibition of aquaporin-4 by zinc. *Biochemistry.* 48:12059–12061.
40. Yukutake, Y., and M. Yasui. 2010. Regulation of water permeability through aquaporin-4. *Neuroscience.* 168:885–891.
41. Silberstein, C., R. Bouley, …, A. N. Van Hoek. 2004. Membrane organization and function of M1 and M23 isoforms of aquaporin-4 in epithelial cells. *Am. J. Physiol. Renal Physiol.* 287:F501–F511.
42. Neely, J. D., B. M. Christensen, …, P. Agre. 1999. Heterotetrameric composition of aquaporin-4 water channels. *Biochemistry.* 38:11156–11163.
43. Hibino, H., and Y. Kurachi. 2007. Distinct detergent-resistant membrane microdomains (lipid rafts) respectively harvest K^+ and water transport systems in brain astroglia. *Eur. J. Neurosci.* 26:2539–2555.
44. Noël, G., D. K. Tham, and H. Moukhles. 2009. Interdependence of laminin-mediated clustering of lipid rafts and the dystrophin complex in astrocytes. *J. Biol. Chem.* 284:19694–19704.
45. Brown, D. A., and E. London. 1998. Functions of lipid rafts in biological membranes. *Annu. Rev. Cell Dev. Biol.* 14:111–136.
46. Simons, K., and E. Ikonen. 1997. Functional rafts in cell membranes. *Nature.* 387:569–572.
47. Tikku, S., Y. Epshtein, …, I. Levitan. 2007. Relationship between Kir2.1/Kir2.3 activity and their distributions between cholesterol-rich and cholesterol-poor membrane domains. *Am. J. Physiol. Cell Physiol.* 293:C440–C450.
48. Ahmed, S. N., D. A. Brown, and E. London. 1997. On the origin of sphingolipid/cholesterol-rich detergent-insoluble cell membranes: physiological concentrations of cholesterol and sphingolipid induce formation of a detergent-insoluble, liquid-ordered lipid phase in model membranes. *Biochemistry.* 36:10944–10953.
49. Baumgart, T., A. T. Hammond, …, W. W. Webb. 2007. Large-scale fluid/fluid phase separation of proteins and lipids in giant plasma membrane vesicles. *Proc. Natl. Acad. Sci. USA*. 104:3165–3170.
50. Kahya, N., D. Scherfeld, …, P. Schwille. 2003. Probing lipid mobility of raft-exhibiting model membranes by fluorescence correlation spectroscopy. *J. Biol. Chem.* 278:28109–28115.
51. Needham, D., and R. S. Nunn. 1990. Elastic deformation and failure of lipid bilayer membranes containing cholesterol. *Biophys. J.* 58:997–1009.
52. Yukutake, Y., S. Tsuji, …, M. Suematsu. 2008. Mercury chloride decreases the water permeability of aquaporin-4-reconstituted proteoliposomes. *Biol. Cell.* 100:355–363.
53. Liu, K., H. Nagase, …, P. Agre. 2006. Purification and functional characterization of aquaporin-8. *Biol. Cell.* 98:153–161.
54. Kozono, D., X. Ding, …, Y. Kitagawa. 2003. Functional expression and characterization of an archaeal aquaporin. AqpM from *Methanothermobacter marburgensis*. *J. Biol. Chem.* 278:10649–10656.
55. Tong, J., M. M. Briggs, …, T. J. McIntosh. 2009. Sorting of lens aquaporins and connexins into raft and nonraft bilayers: role of protein homo-oligomerization. *Biophys. J.* 97:2493–2502.
56. Chen, Jr., P. S., T. Y. Toribara, and H. Warner. 1956. Microdetermination of phosphorous. *Anal. Chem.* 28:1756–1758.
57. Walz, T., B. L. Smith, …, P. Agre. 1994. Biologically active two-dimensional crystals of aquaporin CHIP. *J. Biol. Chem.* 269:1583–1586.
58. Zeidel, M. L., A. Albalak, …, A. Carruthers. 1992. Role of glucose carrier in human erythrocyte water permeability. *Biochemistry.* 31:589–596.
59. Zeidel, M. L., S. V. Ambudkar, …, P. Agre. 1992. Reconstitution of functional water channels in liposomes containing purified red cell CHIP28 protein. *Biochemistry.* 31:7436–7440.
60. Borgnia, M. J., D. Kozono, …, P. Agre. 1999. Functional reconstitution and characterization of AqpZ, the *E. coli* water channel protein. *J. Mol. Biol.* 291:1169–1179.
61. Kai, L., R. Kaldenhoff, …, Z. Xu. 2010. Preparative scale production of functional mouse aquaporin 4 using different cell-free expression modes. *PLoS ONE.* 5:e12972.
62. Yang, B., A. N. van Hoek, and A. S. Verkman. 1997. Very high single channel water permeability of aquaporin-4 in baculovirus-infected

insect cells and liposomes reconstituted with purified aquaporin-4. *Biochemistry.* 36:7625–7632.

63. Carbrey, J. M., D. A. Gorelick-Feldman, …, P. Agre. 2003. Aquaglyceroporin AQP9: solute permeation and metabolic control of expression in liver. *Proc. Natl. Acad. Sci. USA.* 100:2945–2950.

64. Yakata, K., K. Tani, and Y. Fujiyoshi. 2011. Water permeability and characterization of aquaporin-11. *J. Struct. Biol.* 174:315–320.

65. Werten, P. J., L. Hasler, …, P. M. Deen. 2001. Large-scale purification of functional recombinant human aquaporin-2. *FEBS Lett.* 504: 200–205.

66. Kucerka, N., S. Tristram-Nagle, and J. F. Nagle. 2005. Structure of fully hydrated fluid phase lipid bilayers with monounsaturated chains. *J. Membr. Biol.* 208:193–202.

67. Kwok, R., and E. Evans. 1981. Thermoelasticity of large lecithin bilayer vesicles. *Biophys. J.* 35:637–652.

68. Smaby, J. M., H. L. Brockman, and R. E. Brown. 1994. Cholesterol's interfacial interactions with sphingomyelins and phosphatidylcholines: hydrocarbon chain structure determines the magnitude of condensation. *Biochemistry.* 33:9135–9142.

69. Rawicz, W., K. C. Olbrich, …, E. Evans. 2000. Effect of chain length and unsaturation on elasticity of lipid bilayers. *Biophys. J.* 79:328–339.

70. Pan, J., S. Tristram-Nagle, …, J. F. Nagle. 2008. Temperature dependence of structure, bending rigidity, and bilayer interactions of dioleoylphosphatidylcholine bilayers. *Biophys. J.* 94:117–124.

71. Lande, M. B., J. M. Donovan, and M. L. Zeidel. 1995. The relationship between membrane fluidity and permeabilities to water, solutes, ammonia, and protons. *J. Gen. Physiol.* 106:67–84.

72. Gensure, R. H., M. L. Zeidel, and W. G. Hill. 2006. Lipid raft components cholesterol and sphingomyelin increase H^+/OH^- permeability of phosphatidylcholine membranes. *Biochem. J.* 398:485–495.

73. Mathai, J. C., S. Tristram-Nagle, …, M. L. Zeidel. 2008. Structural determinants of water permeability through the lipid membrane. *J. Gen. Physiol.* 131:69–76.

74. Eto, K., Y. Noda, …, S. Sasaki. 2010. Phosphorylation of aquaporin-2 regulates its water permeability. *J. Biol. Chem.* 285:40777–40784.

75. Crane, J. M., and A. S. Verkman. 2009. Reversible, temperature-dependent supramolecular assembly of aquaporin-4 orthogonal arrays in live cell membranes. *Biophys. J.* 97:3010–3018.

76. Furman, C. S., D. A. Gorelick-Feldman, …, J. E. Rash. 2003. Aquaporin-4 square array assembly: opposing actions of M1 and M23 isoforms. *Proc. Natl. Acad. Sci. USA.* 100:13609–13614.

77. Yang, B., and A. S. Verkman. 1997. Water and glycerol permeabilities of aquaporins 1-5 and MIP determined quantitatively by expression of epitope-tagged constructs in *Xenopus* oocytes. *J. Biol. Chem.* 272:16140–16146.

78. Nielsen, C., M. Goulian, and O. S. Andersen. 1998. Energetics of inclusion-induced bilayer deformations. *Biophys. J.* 74:1966–1983.

79. Wiggins, P., and R. Phillips. 2005. Membrane-protein interactions in mechanosensitive channels. *Biophys. J.* 88:880–902.

80. Chang, H. M., R. Reitstetter, …, R. Gruener. 1995. Attenuation of channel kinetics and conductance by cholesterol: an interpretation using structural stress as a unifying concept. *J. Membr. Biol.* 143:51–63.

81. Schmidt, D., and R. MacKinnon. 2008. Voltage-dependent K^+ channel gating and voltage sensor toxin sensitivity depend on the mechanical state of the lipid membrane. *Proc. Natl. Acad. Sci. USA.* 105:19276–19281.

82. Patel, A. J., M. Lazdunski, and E. Honoré. 2001. Lipid and mechano-gated 2P domain K^+ channels. *Curr. Opin. Cell Biol.* 13:422–428.

83. Baenziger, J. E., M. L. Morris, …, S. E. Ryan. 2000. Effect of membrane lipid composition on the conformational equilibria of the nicotinic acetylcholine receptor. *J. Biol. Chem.* 275:777–784.

84. Yuan, C., R. J. O'Connell, …, S. N. Treistman. 2007. Regulation of the gating of BKCa channel by lipid bilayer thickness. *J. Biol. Chem.* 282:7276–7286.

85. Perozo, E., A. Kloda, …, B. Martinac. 2002. Physical principles underlying the transduction of bilayer deformation forces during mechanosensitive channel gating. *Nat. Struct. Biol.* 9:696–703.

86. Lundbaek, J. A., P. Birn, …, O. S. Andersen. 2005. Capsaicin regulates voltage-dependent sodium channels by altering lipid bilayer elasticity. *Mol. Pharmacol.* 68:680–689.

87. Gonen, T., P. Sliz, …, T. Walz. 2004. Aquaporin-0 membrane junctions reveal the structure of a closed water pore. *Nature.* 429:193–197.

88. Harries, W. E., D. Akhavan, …, R. M. Stroud. 2004. The channel architecture of aquaporin 0 at a 2.2-Å resolution. *Proc. Natl. Acad. Sci. USA.* 101:14045–14050.

89. Hite, R. K., Z. Li, and T. Walz. 2010. Principles of membrane protein interactions with annular lipids deduced from aquaporin-0 2D crystals. *EMBO J.* 29:1652–1658.

90. Hite, R. K., T. Gonen, …, T. Walz. 2008. Interactions of lipids with aquaporin-0 and other membrane proteins. *Pflugers Arch.* 456: 651–661.

91. Samuli Ollila, O. H., T. Róg, …, I. Vattulainen. 2007. Role of sterol type on lateral pressure profiles of lipid membranes affecting membrane protein functionality: comparison between cholesterol, desmosterol, 7-dehydrocholesterol and ketosterol. *J. Struct. Biol.* 159:311–323.

92. Cantor, R. S. 1999. Lipid composition and the lateral pressure profile in bilayers. *Biophys. J.* 76:2625–2639.

93. Cantor, R. S. 1997. The lateral pressure profile in membranes: a physical mechanism of general anesthesia. *Biochemistry.* 36:2339–2344.

94. Reference deleted in proof.

95. Cantor, R. S. 1999. The influence of membrane lateral pressures on simple geometric models of protein conformational equilibria. *Chem. Phys. Lipids.* 101:45–56.

96. Aponte-Santamaría, C., R. Briones, …, B. L. de Groot. 2012. Molecular driving forces defining lipid positions around aquaporin-0. *Proc. Natl. Acad. Sci. USA.* 109:9887–9892.

97. Hong, H., and L. K. Tamm. 2004. Elastic coupling of integral membrane protein stability to lipid bilayer forces. *Proc. Natl. Acad. Sci. USA.* 101:4065–4070.

98. Mouritsen, O. G., and M. Bloom. 1984. Mattress model of lipid-protein interactions in membranes. *Biophys. J.* 46:141–153.

99. Nyholm, T. K., S. Ozdirekcan, and J. A. Killian. 2007. How protein transmembrane segments sense the lipid environment. *Biochemistry.* 46:1457–1465.

100. Pilot, J. D., J. M. East, and A. G. Lee. 2001. Effects of bilayer thickness on the activity of diacylglycerol kinase of *Escherichia coli*. *Biochemistry.* 40:8188–8195.

101. Dumas, F., J.-F. Tocanne, …, M. C. Lebrun. 2000. Consequences of hydrophobic mismatch between lipids and melibiose permease on melibiose transport. *Biochemistry.* 39:4846–4854.

102. Israelachvili, J. N. 1977. Refinement of the fluid-mosaic model of membrane structure. *Biochim. Biophys. Acta.* 469:221–225.

103. Lundbaek, J. A. 2008. Lipid bilayer-mediated regulation of ion channel function by amphiphilic drugs. *J. Gen. Physiol.* 131:421–429.

104. Picazo-Juárez, G., S. Romero-Suárez, …, T. Rosenbaum. 2011. Identification of a binding motif in the S5 helix that confers cholesterol sensitivity to the TRPV1 ion channel. *J. Biol. Chem.* 286:24966–24976.

105. Suzuki, H., K. Nishikawa, …, Y. Fujiyoshi. 2008. Formation of aquaporin-4 arrays is inhibited by palmitoylation of N-terminal cysteine residues. *Biochim. Biophys. Acta.* 1778:1181–1189.

106. Levental, I., M. Grzybek, and K. Simons. 2010. Greasing their way: lipid modifications determine protein association with membrane rafts. *Biochemistry.* 49:6305–6316.

107. Linder, M. E., and R. J. Deschenes. 2007. Palmitoylation: policing protein stability and traffic. *Nat. Rev. Mol. Cell Biol.* 8:74–84.

108. Rash, J. E., K. G. Davidson, …, C. S. Furman. 2004. Freeze-fracture and immunogold analysis of aquaporin-4 (AQP4) square arrays, with models of AQP4 lattice assembly. *Neuroscience.* 129:915–934.

109. Verkman, A. S., J. Ratelade, …, L. Tradtrantip. 2011. Aquaporin-4: orthogonal array assembly, CNS functions, and role in Neuromyelitis optica. *Acta Pharmacol. Sin*. 32:702–710.

110. Claudio, L., Y. Kress, …, C. F. Brosnan. 1990. Mechanisms of edema formation in experimental autoimmune encephalomyelitis. The contribution of inflammatory cells. *Am. J. Pathol*. 137:1033–1045.

111. Hirt, L., B. Ternon, …, J. Badaut. 2009. Protective role of early aquaporin 4 induction against postischemic edema formation. *J. Cereb. Blood Flow Metab*. 29:423–433.

112. Namer, I. J., J. Steibel, …, J. Chambron. 1993. Blood-brain barrier breakdown in MBP-specific T cell induced experimental allergic encephalomyelitis. A quantitative in vivo MRI study. *Brain.* 116:147–159.

113. Wolburg-Buchholz, K., A. F. Mack, …, H. Wolburg. 2009. Loss of astrocyte polarity marks blood-brain barrier impairment during experimental autoimmune encephalomyelitis. *Acta Neuropathol*. 118: 219–233.

114. Warth, A., M. Mittelbronn, and H. Wolburg. 2005. Redistribution of the water channel protein aquaporin-4 and the K^+ channel protein Kir4.1 differs in low- and high-grade human brain tumors. *Acta Neuropathol*. 109:418–426.